nature physics

INSIGHT | REVIEW ARTICLES

PUBLISHED ONLINE: 2 APRIL 2012 | DOI: 10.1038/NPHYS2252

Quantum simulations with trapped ions

R. Blatt[1,2]* and C. F. Roos[1,2]

In the field of quantum simulation, methods and tools are explored for simulating the dynamics of a quantum system of interest with another system that is easier to control and measure. Systems of trapped atomic ions can be accurately controlled and manipulated, a large variety of interactions can be engineered with high precision and measurements of relevant observables can be obtained with nearly 100% efficiency. Here, we discuss prospects for quantum simulations using systems of trapped ions, and review the available set of quantum operations and first proof-of-principle experiments for both analog and digital quantum simulations with trapped ions.

The field of quantum information has emerged during the past decade, together with the much refined art of controlling and manipulating quantum systems. Arguably, it is today one of the most lively—and still growing—research areas in physics, with widespread potential applications. The ultimate goal in this field is the realization of a universal quantum computer, promising unprecedented computing power. Reaching that goal, however, will still require many years, if not decades, of improvements in technology and fundamental research. There are, however, no principle roadblocks in sight[1]. Although universal quantum computers for large-scale operations are probably quite a while in the future, research during the past few years has clearly shown that with small numbers of quantum bits (or qubits) a number of applications already become interesting where well controlled quantum systems can be favourably employed. Examples include frequency standards where entangling operations enhance the state detection[2], tests of quantum theory in multiqubit systems[3,4] or the use of qubits as a quantum memory for quantum repeaters.

The power of quantum-information processing is based on the exponentially growing number of computational paths that are available in quantum systems consisting of an increasing number of qubits. Although factoring of large numbers using Shor's algorithm[5] requires tens of thousands of qubits, the use of even small-scale quantum systems may offer a route to efficiently simulate other quantum systems that could be very hard to describe analytically or numerically on classical computers. Such ideas date back to Richard Feynman, who pointed out in his seminal 1981 lecture 'Simulating Physics with Computers' that the proper way of simulating quantum physics would be making use of a quantum machine instead of a classical computer[6]. He conjectured that universal quantum simulators might exist but it was only in 1996 that Seth Lloyd was able to show that universal simulators can indeed be built to efficiently simulate systems with local interactions[7].

Employing one quantum system to simulate the behaviour of another can be realized in two rather distinct ways sketched in Fig. 1: mapping the dynamics of the simulated Hamiltonian to a mathematically equivalent, albeit physically quite different, system emulates a quantum system, and is referred to as an analog quantum simulator[8]. Obviously, the availability of such emulations or analog quantum simulations hinges on the accessibility of a very well controlled quantum system that offers a large variety of interactions that can be precisely controlled. Much more general and even much more challenging, in the spirit of Feynman and Lloyd, is the construction of a universal quantum simulator that can be reprogrammed to accommodate the needs for any system to be investigated. In that case the task is to obtain the solution $|\Psi(t)\rangle$ of the Schrödinger equation describing the action of a time-dependent Hamiltonian $H_{\rm sys}$, which may be written as a sum of many local interactions, on the initial state $|\Psi(0)\rangle$. This, however, requires the use of a freely programmable quantum computer to implement the required Hamiltonians. As was pointed out in ref. 7, the unitary evolution of a system Hamiltonian $H_{\rm sys}$ can be rebuilt by piecewise application of local Hamiltonians $e^{-iH_l t/n}$. According to the Trotter formula[7,9]

$$e^{-iH_{\rm sys}t} \approx \left(e^{-iH_1 t/n} e^{-iH_2 t/n} \ldots e^{-iH_l t/n}\right)^n \qquad (1)$$

the dynamics of the system is then approximated better and better with finer and finer time slices. Equation (1) is applicable for a time-independent Hamiltonian $H_{\rm sys} = \sum_{i=1}^{l} H_i$ but can be easily generalized to time-dependent Hamiltonians. In ref. 7 it was shown that, for any given simulation precision, the complexity of the simulation grows only polynomially with the number of particles to be simulated. Any unitary evolution based on local interactions can thus be simulated; the approach, therefore, provides the basis for universal quantum simulations. Such a quantum simulator, realized by unitaries implemented with a set of universal quantum operations, is referred to as a digital quantum simulator.

During the past decade a large number of technologies have been investigated searching for the optimum technology for an implementation of quantum-information processing[1,10]. Nuclear magnetic resonance in molecules[11] was the first technology used for implementing complex multiqubit gate operations. Although NMR systems are usually considered to be not scalable for general-purpose quantum computation, they have been favourably used for small-scale quantum simulations, both digital and analog[8,12]. Larger systems that lend themselves almost naturally to implement solid-state Hamiltonians[13,14] are available with neutral atoms in optical lattices[15,16]. In these systems, a variety of experimental controls is available to steer the interaction between atoms in the lattice, and with the recently developed techniques for individually addressing single lattice sites[17,18] this method offers a wide range of possibilities for analog simulations[14]. There are a number of other technologies in use for various quantum simulations, such as photons[19–22]; however, their applicability seems to be limited to very small system sizes. Other approaches, such as trapped ions[15,23], resonator-coupled superconducting qubit arrays[24,25] or electron spins in quantum dots or diamond[26], will need to demonstrate that the technology is truly scalable.

[1]Institut für Experimentalphysik, Universität Innsbruck, Technikerstr. 25, A-6020 Innsbruck, Austria, [2]Institut für Quantenoptik und Quanteninformation, Österreichische Akademie der Wissenschaften, Otto-Hittmair-Platz 1, A-6020 Innsbruck, Austria. *e-mail: Rainer.Blatt@uibk.ac.at.

NATURE PHYSICS DOI:10.1038/NPHYS2252

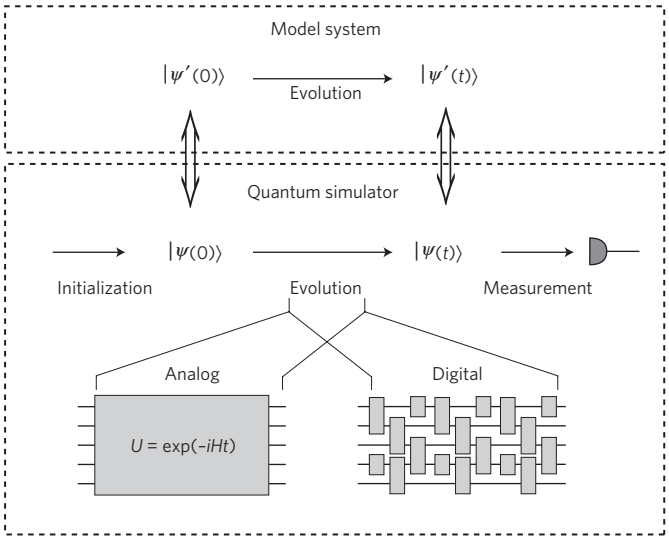

Figure 1 | Principles of quantum simulation. The three main steps of a quantum simulator consist of preparing the input state, evolving it over a time t and carrying out measurements on the evolved state to extract the physical information of interest. The time evolution of the simulator is designed to match the time evolution of the model system to be simulated. In an analog simulator, this is achieved by matching the dynamics of the simulator with the time evolution governing the dynamics of the simulated model. In a digital simulator, the propagator describing the dynamical evolution is constructed from a series of quantum gates. In the illustration, the horizontal lines represent qubits or other elementary constituents of the overall quantum system; grey boxes represent quantum operations acting on the respective constituents covered by the boxes.

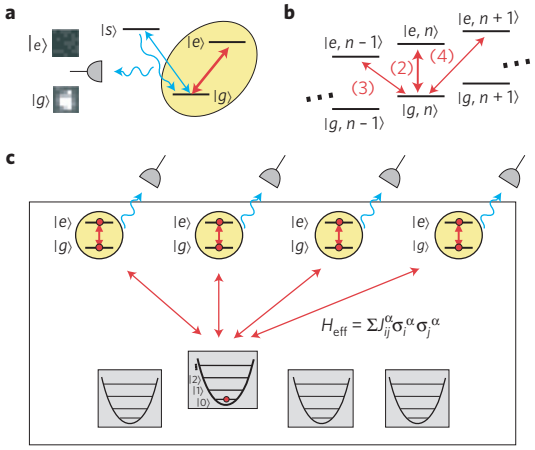

Figure 2 | Trapped-ion quantum system used for quantum-information processing. a, A qubit is encoded in two internal states $|g\rangle, |e\rangle$ of an ion confined in a harmonic potential. Qubit read-out is accomplished by coupling one of the qubit levels to a short-lived state $|s\rangle$. Thus, observation of fluorescence (bright, dark) indicates population of the ground ($|g\rangle$) or excited ($|e\rangle$) state, respectively. The qubit is coherently manipulated by laser pulses coupling states $|g\rangle$ and $|e\rangle$ on either a single- or two-photon transition. **b**, Qubit–motion coupling. The qubit is excited either on the carrier transition (2) or on the sideband transitions (3), (4), which couple it to a vibrational mode. Bracketed numbers refer to equation numbers in the text giving the corresponding Hamiltonians. Excitation on the sideband transitions decreases or increases the vibrational quantum number n on excitation of the qubit. **c**, In an ion crystal, all measurements are made by (spatially resolved) fluorescence detection. The vibrational states can be measured by coupling the ion motion to the qubits using sideband transitions, thus mapping information about the ion motion onto qubits that are subsequently read out. Effective spin–spin interactions are realized by interactions mediated by one or several of the crystal's vibrational modes.

Quantum toolbox with trapped ions

Among the most successful systems investigated for quantum-information processing are well controlled strings of trapped atomic ions held in linear radiofrequency traps[23,27,28]. Present trapped-ion processors are based on qubits encoded in one ion each, and manipulated and made to interact with other qubits by pulses of laser or microwave radiation. Possible electronic qubit states are hyperfine or Zeeman ground states, or a combination of a ground state and an excited metastable electronic state. Depending on the sensitivity of the qubit states to external field noise, the coherence of the qubit state is typically preserved for durations of a few milliseconds up to seconds. A qubit is coherently manipulated by lasers or microwaves resonantly coupling the qubit states as described by the Hamiltonian

$$H_I = \hbar \frac{\Omega}{2} (\sigma^+ e^{i\phi} + \sigma^- e^{-i\phi}) \qquad (2)$$

where the Rabi frequency Ω is controlled by the intensity $I \propto |\Omega|^2$ of the exciting field, ϕ is the phase of the field and $\sigma^{\pm}$ denote the atomic raising and lowering operators. Alternatively, off-resonant couplings can be employed for inducing a.c. Stark shifts described by $H_I = (1/2)\hbar\Omega\sigma_z$. The qubit state is detected by a fluorescence measurement (Fig. 2a) which couples one of the qubit states, but not the other, to a short-lived excited level[29]. In this way, the qubit states are measured by the presence or absence of fluorescence with detection errors as small as 10^{-4} (ref. 30). Qubit rotations before fluorescence detection allow for projective measurements of any spin component. Qubit–qubit correlations are measured by spatially resolved fluorescence detection.

The motion of a trapped ion is composed of harmonic motion along three perpendicular directions. Doppler-cooling techniques enable us to spatially confine the ion to a region much smaller than the optical wavelength[31]. By laser-sideband cooling, a vibrational mode can be prepared in the ground state of the quantum oscillator describing the harmonic motion at low temperature. Reheating times by fluctuating electric fields strongly depend on the ion-trap size, with heating rates ranging between 1 and 10^6 phonons per second[32,33].

As indicated in Fig. 2, narrow-band laser light can be used to couple a qubit, consisting of the two-level system $|g\rangle \equiv |\downarrow\rangle$, $|e\rangle \equiv |\uparrow\rangle$, to the ion motion. The physical basis of the interaction is the momentum transfer from the light field to the ion by stimulated emission or absorption events. The ion motion is described by a quantum harmonic oscillator with states $|n\rangle$, $n = 0, 1, 2, \ldots$ and oscillation frequency ω. The interaction of a qubit with a laser detuned from the qubit transition frequency by $-\omega$ (red sideband) is described by the Hamiltonian

$$H_I^{\text{RSB}} = \hbar \frac{\eta\Omega}{2} i(a\sigma^+ e^{i\phi} - a^\dagger \sigma^- e^{-i\phi}) \qquad (3)$$

Here, creation or destruction of a vibrational quantum is described by the raising or lowering operators, $a^\dagger$ or a, respectively, pertaining to the harmonic oscillator mode; this process goes hand in hand with the respective atomic (de-)excitation. When compared with equation (2), the interaction strength is reduced by a factor $\eta = ka_0$ where k is the overlap of the (effective) wave vector of the electromagnetic wave with the normal vector of the ion motion and a_0 the size of the ion wave packet in the ground state of the harmonic oscillator. Note that this interaction is mathematically equivalent to the interaction of a two-level atom inside a cavity, as described by the Jaynes–Cummings model[34], with the cavity-mode frequency

replaced by the vibrational frequency ω and the interaction strength replaced by $\eta\Omega$. Thus it was realized already in the 1990s that the physics of a trapped-ion system could be used to emulate the dynamics of a cavity quantum electrodynamical (CQED) system[35,36] and of other optical processes[37]. With such operations, CQED physics was simulated in an analog fashion and enabled the creation of highly non-classical states of the ion motion[38], completely equivalent to photonic states in CQED, which are rather hard to prepare and to investigate.

Moreover, interaction with the laser detuned by the trap frequency $+\omega$ (blue sideband) results in another Hamiltonian

$$H_I^{\mathrm{BSB}} = \hbar\frac{\eta\Omega}{2} i(a^\dagger \sigma^+ \mathrm{e}^{i\phi} - a\sigma^- \mathrm{e}^{-i\phi}) \qquad (4)$$

which is not available in CQED physics, but provides for a further route to simulate quantum systems. In addition to providing operations entangling qubit and motion, the Hamiltonians (3) and (4) are also crucial for measuring the vibrational quantum state by unitary operations mapping the relevant information onto the qubit which is subsequently read out[38–40].

Ion crystals are created by laser cooling an ensemble of ions into the submillikelvin range. At the equilibrium positions of the ions, the Coulomb repulsion between the ions is balanced by the trap confinement force. Typically, the ion oscillation frequencies $\omega_i/(2\pi)$, $i = x, y, z$, are about 1–10 MHz. In linear ion traps[41], the axial potential can be made much less confining than the transverse one. In such strongly anisotropic potentials, linear ion crystals form with distances d between neighbouring ions in the range of a few micrometres. This enables the detection of individual ions and their manipulation by strongly focused laser beams. For a laser-cooled N-ion crystal, the ion motion around the equilibrium positions is described by a set of $3N$ collective vibrational modes with distinct oscillation frequencies. These motional degrees of freedom form part of the quantum system available for quantum simulations.

Deterministic operations entangling qubits among one another can be realized by Coulomb-mediated interactions of laser pulses exciting the ions on the red and blue sidebands of these collective modes. Different schemes have been proposed and experimentally demonstrated, based on laser beams that either subsequently interact with single ions[23,42] or couple to all qubits at the same time[43–46]. The latter interactions can be described by effective Hamiltonians inducing spin–spin interactions $\sigma_i^z \otimes \sigma_j^z$ or $\sigma_i^\phi \otimes \sigma_j^\phi$ between all pairs of ions (i,j) participating in the interaction where $\sigma_j^\phi = \cos\phi\sigma_j^x + \sin\phi\sigma_j^y$ and σ_j^k denotes the Pauli matrix σ^k acting on the j th qubit. These entangling interactions are independent of the vibrational state to first order[47], which makes them attractive for simulating spin–spin interactions[48]. Here and later on, Pauli spin matrices are used to describe operations acting on the pseudo-spin system composed of the two qubit states. This pseudo-spin should not be mistaken for the atomic spin.

Analog quantum simulations with trapped ions

The flexibility in engineering interactions between the set of qubits and harmonic oscillators constituting the trapped ions' quantum system enables the construction of a wide range of Hamiltonians. Instead of trying to review all proposals dealing with analog quantum simulations in trapped ions (many proposals are summarized in ref. 49), in this section we shall focus on two examples where first experimental steps have been taken.

Quantum spin systems serve as models for modelling magnetism in condensed matter. However, understanding these quantum many-body systems is challenging, and, as numerical simulation techniques can become computationally too demanding even for systems consisting of a few tens of spins[50,51], quantum simulation might offer new insights into the physics of these systems.

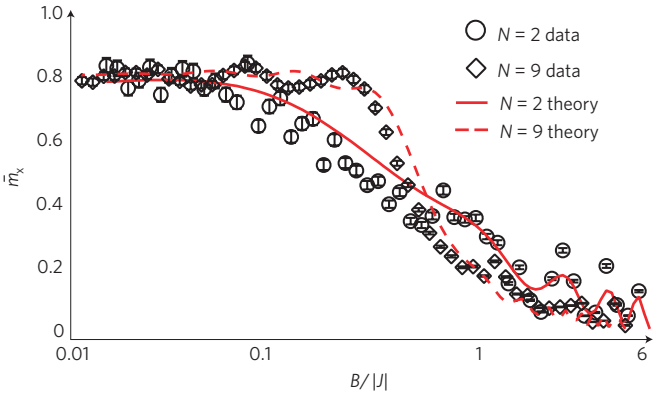

Figure 3 | Magnetization data. The magnetization $\overline{m}_x = \sum_{i=1}^{N}\langle\sigma_i^x\rangle/N$ (as derived from the populations of the individual two-level systems that represent the simulated spins, for details see ref. 57) for $N = 2$ spins (circles) is contrasted with that of $N = 9$ spins (diamonds), with representative error bars for the detection process[57]. The data deviate from unity at $B/|J| = 0$ by ~20%, predominantly owing to decoherence from spontaneous emission in Raman transitions and further dephasing from Raman beam intensity fluctuations[57]. The theoretical time-evolution curves (solid line for $N = 2$ and dashed line for $N = 9$ spins) are calculated by averaging over 10,000 quantum trajectories. Reproduced from ref. 57.

The simulation of quantum spin systems with trapped ions was proposed in ref. 48. In that model, each ion of a trapped ion crystal encodes a spin-1/2 system. The spin Hamiltonian

$$H = \frac{1}{2}\sum_{\alpha,i,j} J_{ij}^\alpha \sigma_i^\alpha \sigma_j^\alpha + \sum_{\alpha,i} B^\alpha \sigma_i^\alpha \qquad (5)$$

is realized by lasers interacting with all qubits representing the spins and coupling them with one another and to a fictitious magnetic field B^α. Here, the spin–spin interactions are effective interactions arising from off-resonant coupling to the motional sidebands (3), (4) in a regime where the ion–motion coupling strength is much smaller than the detuning of the lasers. In this limit, the motional state stays close to its initial state and the vibrational degrees of freedom can be adiabatically eliminated. Similar interactions are used for entangling quantum gates based on spin-dependent forces[43,45], where, however, much stronger transient excitations of the motional state occur. To engineer the Hamiltonian (5), a pair of laser beams is required for realizing each component $\sigma_i^\alpha\sigma_j^\alpha$, $\alpha = x, y, z$, of the spin–spin term, and another laser is needed for generating the coupling to the magnetic field. The spin–spin coupling constants J_{ij}^α depend on the laser detuning which determines the coupling strengths to the different normal mode of the ion motion. An implementation of the Hamiltonian (5) on the basis of microwave transitions in inhomogeneous magnetic fields[52] will be discussed later.

A proof-of-principle experiment with two ions was carried out in 2008 (ref. 53), demonstrating an adiabatic evolution from paramagnetic to ferromagnetic order when ramping up an Ising-interaction term in the presence of a transverse field. Experiments simulating a quantum Ising model with transverse field with three ions demonstrated the control over the nearest- and next-nearest-neighbour coupling and its effect on different magnetic ordering, including spin frustration[54–56]. More recently, such experiments have been extended to linear strings of $N = 3\ldots9$ ions[57,58], where the observed sharpening of the crossover from paramagnetic to ferromagnetic order with increasing ion number is the precursor of a quantum phase transition in the limit $N \to \infty$. Figure 3,

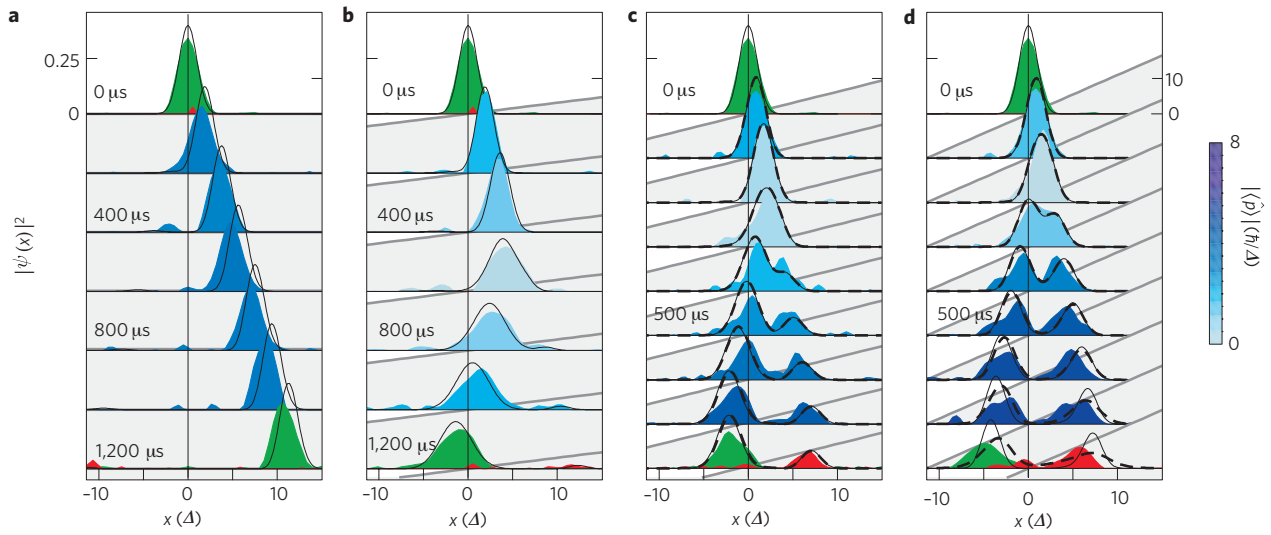

Figure 4 | Quantum simulation of relativistic scattering (Klein tunnelling) for linear potentials. Particle–wave packets (filled curves), presented in units of the size of the ground-state wavefunction, Δ, are compared with ideal predictions (solid black lines) and predictions taking corrections to the Lamb–Dicke approximation into account (dashed black lines). In the first and last frames of each sequence the positive (green)- and negative (red)-energy components are reconstructed separately. The blue colour scale of these panels represents the measured expectation value of momentum. The axis on the right shows the potential energy in units of initial kinetic energy. **a**, Without a potential, the particle moves to the right with constant velocity. **b**–**d**, For a shallow potential gradient (**b**) the particle is almost completely reflected, and for steeper gradients (**c**,**d**) part of the wave packet propagates into the repulsive potential through Klein tunnelling. Figure reproduced with permission from ref. 71, © 2011 APS.

taken from ref. 57, shows the result of such an experiment. In this measurement, the arising magnetism in a fully connected non-uniform ferromagnetic quantum Ising model implemented with up to nine trapped $^{171}Yb^{+}$ ions is simulated[57]. When increasing the Ising coupling strengths relative to the transverse field, the spin ordering changes from paramagnetic to ferromagnetic, indicating a phase transition, which sharpens as more ions are used for the simulation. More information about the simulation of spin systems can be found in a recent review[59]. To become competitive with classical simulation techniques, trapped-ion simulations of spin systems will have to demonstrate simulations with larger numbers of spins and more complex spin–spin couplings J_{ij}^{α}. Then, even for fairly small numbers of spins, rich phase diagrams with sharp transitions have been predicted[60]. Experiments along these lines will require coupling to multiple vibrational modes[48] and most probably also two-dimensional trapping geometries, topics that will be briefly touched on at the end of this Review.

Quantum simulations with trapped ions are not limited to the domain of low-energy physics. Proposals have been put forward for simulating relativistic quantum particles[61], Hawking radiation[62–65] and particle generation[66] using analog trapped-ion simulators. Here, we illustrate how a single laser-cooled ion can be made to behave like a relativistic quantum particle.

At submillikelvin temperatures, the quantum dynamics of a trapped ion is adequately described by the Schrödinger equation $i\hbar\partial\psi/\partial t = H\psi$. Therefore, to simulate a relativistic particle, the Schrödinger Hamiltonian H has to be engineered such that it matches the Hamiltonian $H_{\mathrm{D}} = c\,\boldsymbol{\alpha}\cdot\hat{\mathbf{p}} + \beta mc^2$ of the Dirac equation governing the dynamics of the particle to be simulated. Here, $\boldsymbol{\alpha}$ and β are the Dirac matrices and $\hat{\mathbf{p}}$ the momentum operator. For the simulation of a free Dirac particle, it was proposed in ref. 61 to encode the four-component spinor state ψ in four internal states of the ion and to simulate the Dirac Hamiltonian H_{D} by laser–ion interactions coupling the internal states among one another and to the three harmonic oscillators describing the ion motion in the trap.

In the experiment described in ref. 67, this proposal is realized for a Dirac equation in $1+1$ dimensions. In this case, the spinors have only two components that were encoded in two long-lived levels of a $^{40}Ca^{+}$ ion, and the Hamiltonian $H_{\mathrm{D}} = c\,\hat{p}\,\sigma_x + mc^2\,\sigma_z$ is realized by spin-dependent light forces and a.c. Stark shifts. In addition to simulating free Dirac particles, particles in linear and quadratic potentials can also be simulated by adding a potential generated by laser excitation of a second particle[68]. With these tools, phenomena analogous to relativistic quantum effects such as 'Zitterbewegung'—the trembling motion of a Dirac particle predicted by Schrödinger[69]—and Klein tunnelling[70] can be investigated in trapped-ion experiments[67,71].

For the observation of the simulated quantum dynamics, schemes for measuring observables of interest are required. Information about the motional state needs to be mapped onto the internal states of the ion, where it is read out by fluorescence detection. Instead of completely characterizing the motional state by tomographic techniques[39,72], it is more efficient to measure the centre-of-mass position $\langle\hat{x}\rangle$ of the ion[73] or its probability distribution $\langle\delta(\hat{x}-x)\rangle$ (refs 40,74) in position space by tailored detection schemes.

The motion of a relativistic wavepacket in the presence of a potential was simulated by Gerritsma and colleagues[71]. For this, one ion was used to simulate the Dirac particle and a second ion to simulate the action of a linear potential on the Dirac particle. Figure 4 shows the simulated behaviour of the wavepacket in that potential: in the absence of a potential (Fig. 5a), the motion of a free particle is observed, for small slopes (Fig. 5b; non-relativistic limit) the wavepacket is reflected and for steeper slopes (Fig. 5c,d; relativistic scattering) the positive-energy part of the wavefunction (simulated matter) is reflected and the negative-energy part of the wavefunction (simulated antimatter) is transmitted, which corresponds to a quantum simulation of Klein tunnelling[71].

The experiments described above all deal with a single relativistic particle and thus do not present insurmountable obstacles to analytic calculation or conventional simulation techniques. To bring these experiments to a new level of complexity will require the development of techniques for the simulation of quantum fields[64–66,75] that allow for the creation and annihilation of particles.

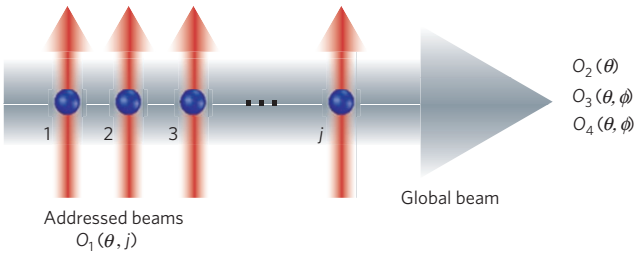

Figure 5 | Quantum toolbox with a string of trapped ions. Laser beams interact with the ion(s) for a predetermined time, corresponding to phases θ in units of π. For this, the ions are either simultaneously (global beam) or individually (local beam) addressed to implement the toolbox operations $O_1(\theta, j)$ (local), $O_2(\theta)$ and $O_3(\theta, \phi)$ (global) and the entangling $O_4(\theta, \phi)$ (global). These operations are applied sequentially according to a given simulation (or computational) task.

Digital quantum simulations with trapped ions

In the digital approach to quantum simulation, the state of the system to be simulated is encoded in a quantum register of the simulator and the dynamics is approximated with a stroboscopic sequence of quantum gates. This approach is very flexible as it enables us in principle to efficiently simulate any local quantum system[7]. Such a universal quantum simulator is an instance of a special-purpose quantum computer. Quantum error-correction techniques to correct for and quantitatively bound experimental errors are therefore available in large-scale digital quantum simulations. Efficiency considerations with respect to the desired simulation precision are discussed in refs 12,76.

Any universal set of quantum gates can be the basis for the operations of a digital quantum simulator. The digital approach has been experimentally explored with NMR systems and with trapped ions. Here, we shall illustrate it by describing a recent experiment using the Trotter technique for simulating spin–spin interactions in a string of two to six $^{40}Ca^{+}$ ions[77] where the qubits are encoded in superpositions of the $|S_{1/2}\rangle$ ground and $|D_{5/2}\rangle$ metastable states of the calcium ion. Then, states encoded in these qubits are manipulated by laser pulses implementing the following universal set of operations[78]: $O_1(\theta, j) = \exp(-i\theta\sigma_j^z)$, $O_2(\theta) = \exp(-i\theta\sum_i \sigma_i^z)$, $O_3(\theta, \phi) = \exp(-i\theta\sum_i \sigma_i^\phi)$ and $O_4(\theta, \phi) = \exp(-i\theta\sum_{i<j} \sigma_i^\phi \sigma_j^\phi)$. As indicated in Fig. 5, O_1 is realized by a strongly focussed beam interacting with the jth ion, whereas O_2–O_4 are implemented with a second beam that couples to all ions with the same strength. The entangling operation O_4 is realized by off-resonant coupling to a vibrational mode as described earlier.

The digital approach enables arbitrary interactions between spins to be programmed. For simulations shown in Figs 6 and 7, we define dimensionless Hamiltonians $\tilde{H}$, that is $H = E\tilde{H}$ such that $U = e^{-i\tilde{H}Et/\hbar}$ and the system evolution is quantified by a unitless phase $\theta = Et/\hbar$.

According to (1), and as detailed in ref. 77, the Hamiltonians to be simulated are piecewise applied using the toolbox operations given above. The dynamics of the system is then implemented with a stroboscopic sequence of O_i $(i = 1, 2, 3, 4)$ gates, representing for example the magnetic field and spin–spin evolution operators for Ising-type interactions. As was shown in ref. 77, the simulated dynamics converge closer to the exact dynamics as the digital resolution is increased.

Figure 6a–c shows the simulated dynamics of two-spin systems with increasing complexity and the initial state $|{\rightarrow}{\leftarrow}\rangle_x \equiv (|{\downarrow}\rangle + |{\uparrow}\rangle)(|{\downarrow}\rangle - |{\uparrow}\rangle)$. Figure 6a shows the state evolution for the Ising system, where the operations $C = O_2(\pi/16)$ and $D = O_4(\pi/16, 0)$ are employed to implement the uniform field B and the interaction

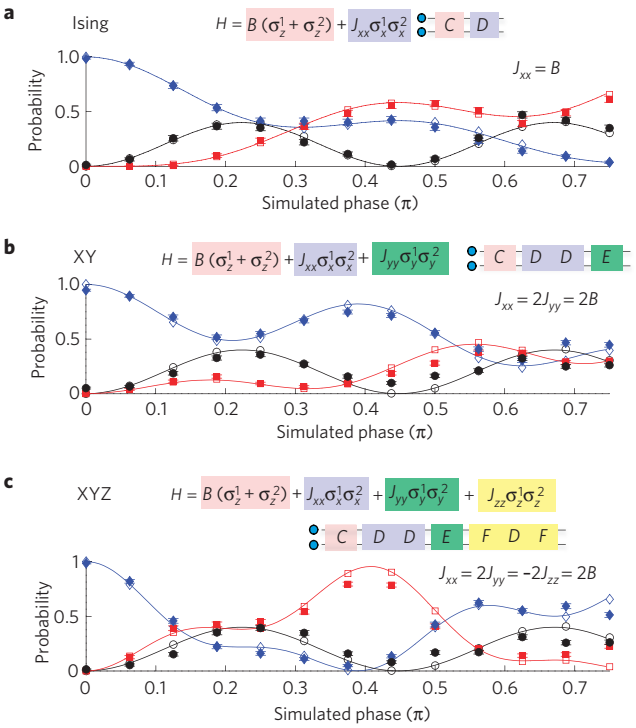

Figure 6 | Digital simulations of a two-spin system interacting through Ising, XY and XYZ interaction plus a transverse field. Dynamics of the initial state $|{\rightarrow}{\leftarrow}\rangle_x$ using a fixed digital resolution of $\pi/16$. Each panel shows how a single digital step is built from the elementary interactions: $C = O_2(\pi/16)$, $D = O_4(\pi/16, 0)$, $E = O_4(\pi/16, \pi)$, $F = O_3(\pi/4, 0)$. Lines show exact dynamics induced by the respective Hamiltonian, open symbols the ideal digitized dynamics. Filled symbols are measured data (blue diamond, $\rightarrow\leftarrow_x$; red square, $\leftarrow\rightarrow_x$; black circle, $\leftarrow\leftarrow_x, \rightarrow\rightarrow_x$). Figure adapted with permission from ref. 77, © 2011 AAAS.

J, respectively. More complex systems with further spin–spin interactions in the y ('XY' model) and z ('XYZ' model) directions can be simulated by reprogramming the operation sequence. The dynamics due to a further spin–spin interaction in the y direction is simulated by adding another entangling operation (labelled E in Fig. 6b) to each step of the Ising stroboscopic sequence. To simulate a Heisenberg interaction, a third spin–spin interaction in the z direction is realized by adding yet another entangling gate sandwiched between a pair of collective single-qubit operations set to rotate the reference frame of the qubits. In the simulated dynamics of the initial state $|{\rightarrow}{\leftarrow}\rangle_x$ under each model, for a fixed digital resolution of $\theta/n = \pi/16$ and 12 Trotter steps, 24, 48 and 84 gates are used for the Ising, XY and XYZ simulations, respectively.

As an even more complex example, Fig. 7a shows the observed dynamics of the four-spin state $|{\uparrow}{\uparrow}{\uparrow}{\uparrow}\rangle \equiv |eeee\rangle$ under a long-range Ising-type interaction. The rich structure of the dynamics reflects the increased complexity of the underlying Hamiltonian: oscillation frequencies correspond to the energy gaps in the spectrum. This information can be extracted through a Fourier transform of the data[77]. Figure 7b shows the observed dynamics for the largest simulation presented in ref. 77: a six-spin many-body interaction, which directly couples the states $|{\uparrow}{\uparrow}{\uparrow}{\uparrow}{\uparrow}{\uparrow}\rangle$ and $|{\downarrow}{\downarrow}{\downarrow}{\downarrow}{\downarrow}{\downarrow}\rangle$, periodically producing a maximally entangled Greenberger–Horne–Zeilinger state.

The toolbox above can be extended to include optical pumping techniques and thus enables simulations of non-Hermitian Hamiltonians and therefore of open quantum systems as well[79].

NATURE PHYSICS DOI:10.1038/NPHYS2252

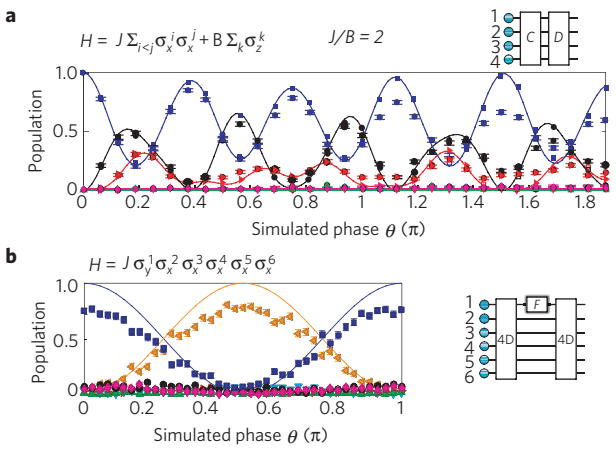

Figure 7 | Digital simulations of four- and six-spin systems. Dynamics of the initial state where all spins point up. **a**, Four-spin long-range Ising system. Each digital step is $D.C = O_4(\pi/16, 0).O_2(\pi/32)$. Error bars are smaller than the point size. **b**, Six-spin six-body interaction. $F = O_1(\theta, 1)$, $4D = O_4(\pi/4, 0)$. Lines, exact dynamics. Open symbols, ideal digitized. Filled symbols, data (blue square, P_0; magenta diamond, P_1; black circle, P_2; green triangle, P_3; red right triangle, P_4; cyan down triangle, P_5; orange left triangle, P_6, where P_i is the total probability of finding i spins pointing down). Figure reproduced with permission from ref. 77, © 2011 AAAS.

New directions

All the experiments described so far involve linear strings of ions held in harmonic traps and subject to spin-dependent forces induced by laser beams. Although this set-up will continue to play a key role in future experiments, there are also various new approaches being explored at present. Here, we shall discuss a couple of ideas that address new ways of coupling ions, handling larger numbers of ions and modifying the geometrical arrangement in which the ions are held.

An alternative to optical spin-dependent forces for entanglement creation is the use of microwaves. As the momentum transfer by absorption or emission of free-space microwave photons is too small to be useful, magnetic-field gradients provide a means of creating spin-dependent potentials for exhibiting a differential Zeeman shift[52] or driving sideband transitions[80]. Experiments have demonstrated a coupling between two internal states of an ion and its motion using either static[81] or oscillating field gradients[82]. The latter have been recently used for entangling a pair of ions by inducing correlated spin flips[82,83]. Quantum simulations of spin systems based on forces generated by magnetic-field gradients would have much less stringent low-temperature requirements than their laser-based counterparts. To achieve substantial ion–ion couplings, large field gradients of about 10–100 T m^{-1} are required, which can be achieved in microfabricated ion traps with current-carrying structures in close proximity to the ions[82,84,85].

Microfabricated ion traps are also of interest in other respects, as they offer greater flexibility in shaping the external trapping potential, compared with the standard Paul traps. When scaling up quantum simulations with long strings of ions held in harmonic potentials, the ratio of transverse to axial trap frequencies has to grow as $\omega_{x,y}/\omega_z > 0.77N/\sqrt{\log N}$ with the number of ions N, to prevent the ion string from undergoing a transition change to a zigzag configuration[86]. This sets a technical upper limit to the number of ions in a linear configuration. If, however, anharmonic terms are added to the axial potentials to keep the ion distance d constant over the length of the ion string, the ion string retains its linear structure for transverse frequencies $\omega_{x,y} > 2.05\sqrt{e^2/(4\pi\epsilon_0 m d^3)}$ (refs 86,87), where m denotes the ion mass and ϵ_0 the vacuum permittivity. Good approximations to the required axial potential can be achieved in a segmented trap with a small number of control electrodes[88]. If long strings of ions are trapped in such an anharmonic potential, there will be low-frequency axial modes with substantial thermal excitation that will be difficult to laser-cool close to the ground state. For this reason, spin–spin couplings will most likely be engineered by coupling to the transverse modes, which have a small frequency spread $\Delta\omega$. This would allow for simulations of short-range spin–spin interactions mediated by electromagnetic forces coupling spin and motion with a detuning much bigger than $\Delta\omega$.

Another path to quantum simulations with larger numbers of ions makes use of microtraps for realizing two-dimensional trapping geometries by placing each ion into a minimum of the trapping potential[89–94]. With two-dimensional ion crystals at hand, quantum simulation of spin–boson models[95], phonon superfluids[96], spin frustration[97] or the study of edge states of topological insulators[98] could be carried out. The big challenge when trapping ions in individual traps is to achieve sizeable (state-dependent) couplings between the ions, as the Coulomb-mediated motional coupling between them scales as $\omega^{-1}d^{-3}$ with the trap frequency ω and ion distance d. This approach requires potential variations on length scales well below 100 μm. Only recently, first experiments have demonstrated coherent coupling of ions trapped in the two wells of a double-well potential[99,100]. An alternative to trapping each ion separately for simulating two-dimensional spin frustration might be to use zigzag crystals or the coupling of linear crystals held in separate traps[85,101]. As an alternative to Coulomb-mediated ion–ion interactions, the use of dipole–dipole interactions between Rydberg ions has been proposed[102,103].

All approaches described above are based on ions trapped by means of radiofrequency fields. This, however, is not the only way of trapping ions. In Penning traps, the crystallization of hundreds of ions in a planar crystal has been demonstrated[104]; the ion motion can be excited with state-dependent optical dipole forces[105]. If a similar level of control over the ions as was demonstrated in radiofrequency traps could be achieved in these traps, they would become an attractive system for the simulation of two-dimensional spin systems[97].

Trapping ions by optical forces[106] is another way of creating strongly anharmonic potentials with prospects for simulations aiming at simulating the Frenkel–Kontorova model and friction[107,108]. Also, optical forces might be of interests in quantum simulations involving ions and neutral atoms[109,110].

Summary and outlook

The progress in quantum-information processing over the past decade has opened up exciting new perspectives for the realization of quantum simulations. Among the systems investigated, trapped ions have proved to be one of the best, enabling both reliable quantum control and measurements with high fidelity. Most recent experimental results on quantum simulations with trapped ions have been summarized and reviewed, and a number of further potential applications have been indicated. The current efforts towards scalable ion trap systems, both for long strings of ions and two-dimensional ion arrays, offer promising tools for future experiments. With these at hand, it will be necessary to demonstrate in the not-too-distant future—at least on a proof-of-principle level—that quantum simulations will be able to go beyond what can be done with classical computers. At this time, simulating the dynamics of spin Hamiltonians of the Ising type with general interactions and more than 40 ions seems to be a problem that goes beyond the classical capabilities[111] and that may be in reach within the next few years for trapped-ion experiments.

Also, for much-extended quantum simulations and for high (or higher) precision, the influence of errors on the simulation result is an important topic; at present, the question of whether simulator imperfections will have a substantial impact or not on quantities of interest to be extracted from the simulation has not been studied in depth[112]. For analog quantum systems, techniques such as encoding into decoherence-free subspaces[113] or the application of dynamical decoupling techniques[114] might be needed to suppress unwanted decoherence, and thus to stabilize the simulation processes. For digital quantum simulations, quantum-error-correction techniques[115] are likely to be required, albeit at the expense of much-increased experimental overhead. However, the necessity for error correction depends also on the problem to be simulated. For example, simulated phase transitions may be visible with only marginal error correction, whereas the precise simulation, for example, of molecular potentials or energy gaps of a spin system presumably requires much more involved error correction or error-avoiding protocols.

Finally, for large quantum simulations that go beyond classical computing, verification of the results will become an issue. It is often argued that this may be the bottleneck for quantum simulations. However, this is not the case when several different devices with possibly different technologies become available to run the same simulations. Then large-scale quantum simulations can be compared with one another—in the same way as has happened for metrological precision experiments for defining, for example, the second as an International System of Units (SI) unit. Therefore, quantum simulations can be considered a new method of precision spectroscopy and quantum metrology that is able to tackle both fundamental and applied questions.

References

1. Zoller, P. *et al.* Quantum information processing and communication. Strategic report on current status, visions and goals for research in Europe. *Eur. Phys. J. D* **36,** 203–228 (2005).
2. Schmidt, P. O. *et al.* Spectroscopy using quantum logic. *Science* **309,** 749–752 (2005).
3. Weihs, G., Jennewein, T., Simon, C., Weinfurter, H. & Zeilinger, A. Violation of Bell's inequality under strict Einstein locality conditions. *Phys. Rev. Lett.* **81,** 5039–5043 (1998).
4. Rowe, M. A. *et al.* Experimental violation of a Bell's inequality with efficient detection. *Nature* **409,** 791–794 (2001).
5. Shor, P. W. *Proc. 35th Annual Symposium on Foundations of Computer Science* 124–134 (IEEE Computer Soc. Press, 1994).
6. Feynman, R. Simulating physics with computers. *Int. J. Theoret. Phys.* **21,** 467–488 (1982).
7. Lloyd, S. Universal quantum simulators. *Science* **273,** 1073–1078 (1996).
8. Buluta, I. & Nori, F. Quantum simulators. *Science* **326,** 108–111 (2009).
9. Trotter, H. F. On the product of semi-groups of operators. *Proc. Am. Math. Soc.* **10,** 545–551 (1959).
10. Army Research Office *ARDA Quantum Computation Roadmap* (Los Alamos National Laboratory, 2005), available at http://qist.lanl.gov/qcomp_map.shtml.
11. Vandersypen, L. M. K. & Chuang, I. L. NMR techniques for quantum control and computation. *Rev. Mod. Phys.* **76,** 1037–1069 (2005).
12. Brown, K. L., Munro, W. J. & Kendon, V. M. Using quantum computers for quantum simulation. *Entropy* **12,** 2268–2307 (2010).
13. Jaksch, D., Bruder, C., Cirac, J. I., Gardiner, C. W. & Zoller, P. Cold bosonic atoms in optical lattices. *Phys. Rev. Lett.* **81,** 3108–3111 (1998).
14. Lewenstein, M. *et al.* Ultracold atomic gases in optical lattices: Mimicking condensed matter physics and beyond. *Adv. Phys.* **56,** 243–379 (2007).
15. Jane, E., Vidal, G., Dür, W., Zoller, P. & Cirac, J. I. Simulation of quantum dynamics with quantum optical systems. *Quant. Inf. Comp.* **3,** 15–37 (2003).
16. Bloch, I., Dalibard, J. & Nascimbéne, S. Quantum simulations with ultracold quantum gases. *Nature Phys.* **8,** 267–276 (2012).
17. Bakr, W. S., Gillen, J. I., Peng, A., Fölling, S. & Greiner, M. A quantum gas microscope for detecting single atoms in a Hubbard-regime optical lattice. *Nature* **462,** 74–77 (2009).
18. Sherson, J. F. *et al.* Single-atom-resolved fluorescence imaging of an atomic Mott insulator. *Nature* **467,** 68–72 (2010).
19. O'Brien, J. L. Optical quantum computing. *Science* **318,** 1567–1570 (2007).
20. Lanyon, B. P. *et al.* Towards quantum chemistry on a quantum computer. *Nature Chem.* **2,** 106–111 (2010).
21. Ma, X., Dakic, B., Naylor, W., Zeilinger, A. & Walther, P. Quantum simulation of the wavefunction to probe frustrated Heisenberg spin systems. *Nature Phys.* **7,** 399–405 (2011).
22. Aspuru-Guzik, A. & Walther, P. Photonic quantum simulators. *Nature Phys.* **8,** 285–291 (2012).
23. Cirac, J. I. & Zoller, P. Quantum computations with cold trapped ions. *Phys. Rev. Lett.* **74,** 4091–4094 (1995).
24. Schoelkopf, R. J. & Girvin, S. M. Wiring up quantum systems. *Nature* **451,** 664–669 (2008).
25. Houck, A. A., Türeci, H. E. & Koch, J. On-chip quantum simulation with superconducting circuits. *Nature Phys.* **8,** 292–299 (2012).
26. Hanson, R. & Awschalom, D. D. Coherent manipulation of single spins in semiconductors. *Nature* **453,** 1043–1049 (2008).
27. Blatt, R. & Wineland, D. Entangled states of trapped atomic ions. *Nature* **453,** 1008–1015 (2008).
28. Häffner, H., Roos, C. F. & Blatt, R. Quantum computing with trapped ions. *Phys. Rep.* **469,** 155–203 (2008).
29. Nagourney, W., Sandberg, J. & Dehmelt, H. Shelved optical electron amplifier: Observation of quantum jumps. *Phys. Rev. Lett.* **56,** 2797–2799 (1986).
30. Myerson, A. H. *et al.* High-fidelity readout of trapped-ion qubits. *Phys. Rev. Lett.* **100,** 200502 (2008).
31. Leibfried, D., Blatt, R., Monroe, C. & Wineland, D. Quantum dynamics of single trapped ions. *Rev. Mod. Phys.* **75,** 281–324 (2003).
32. Turchette, Q. A. *et al.* Heating of trapped ions from the quantum ground state. *Phys. Rev. A* **61,** 063418 (2000).
33. Deslauriers, L. *et al.* Scaling and suppression of anomalous heating in ion traps. *Phys. Rev. Lett.* **97,** 103007 (2006).
34. Jaynes, E. T. & Cummings, F. W. Comparison of quantum and semiclassical radiation theories with application to the beam maser. *Proc. IEEE* **51,** 89–109 (1963).
35. Blockley, C. A., Walls, D. F. & Risken, H. Quantum collapses and revivals in a quantized trap. *Europhys. Lett.* **17,** 509–514 (1992).
36. Cirac, J. I., Blatt, R., Parkins, A. S. & Zoller, P. Quantum collapse and revival in the motion of a single trapped ion. *Phys. Rev. A* **49,** 1202–1207 (1994).
37. Wineland, D. J. *et al.* Trapped ion quantum simulator. *Proc. Am. Math. Soc.* **T76,** 147–151 (1998).
38. Meekhof, D. M., Monroe, C., King, B. E., Itano, W. M. & Wineland, D. J. Generation of nonclassical motional states of a trapped atom. *Phys. Rev. Lett.* **76,** 1796–1799 (1996).
39. Leibfried, D. *et al.* Experimental determination of the motional quantum state of a trapped atom. *Phys. Rev. Lett.* **77,** 4281–4285 (1996).
40. Zähringer, F. *et al.* Realization of a quantum walk with one and two trapped ions. *Phys. Rev. Lett.* **104,** 100503 (2010).
41. Raizen, M. C., Bergquist, J. C., Gilligan, J. M., Itano, W. M. & Wineland, D. J. Linear trap for high-accuracy spectroscopy of stored ions. *J. Mod. Opt.* **39,** 233–242 (1992).
42. Schmidt-Kaler, F. *et al.* Realization of the Cirsac–Zoller controlled-NOT quantum gate. *Nature* **422,** 408–411 (2003).
43. Sørensen, A. & Mølmer, K. Quantum computation with ions in thermal motion. *Phys. Rev. Lett.* **82,** 1971–1974 (1999).
44. Sackett, C. A. *et al.* Experimental entanglement of four particles. *Nature* **404,** 256–259 (2000).
45. Leibfried, D. *et al.* Experimental demonstration of a robust, high-fidelity geometric two ion-qubit phase gate. *Nature* **422,** 412–415 (2003).
46. Benhelm, J., Kirchmair, G., Roos, C. F. & Blatt, R. Towards fault-tolerant quantum computing with trapped ions. *Nature Phys.* **4,** 463–466 (2008).
47. Kirchmair, G. *et al.* Deterministic entanglement of ions in thermal states of motion. *New J. Phys.* **11,** 023002 (2009).
48. Porras, D. & Cirac, J. I. Effective quantum spin systems with trapped ions. *Phys. Rev. Lett.* **92,** 207901 (2004).
49. Johanning, M., Varón, A. F. & Wunderlich, C. Quantum simulations with cold trapped ions. *J. Phys. B* **42,** 154009 (2009).
50. Troyer, M. & Wiese, U-J. Computational complexity and fundamental limitations to fermionic quantum Monte Carlo simulations. *Phys. Rev. Lett.* **94,** 170201 (2005).
51. Sandvik, A. W. Ground states of a frustrated quantum spin chain with long-range interactions. *Phys. Rev. Lett.* **104,** 137204 (2010).
52. Mintert, F. & Wunderlich, C. Ion-trap quantum logic using long-wavelength radiation. *Phys. Rev. Lett.* **87,** 257904 (2001).
53. Friedenauer, H., Schmitz, H., Glueckert, J., Porras, D. & Schaetz, T. Simulating a quantum magnet with trapped ions. *Nature Phys.* **4,** 757–761 (2008).
54. Kim, K. *et al.* Entanglement and tunable spin–spin couplings between trapped ions using multiple transverse modes. *Phys. Rev. Lett.* **103,** 120502 (2009).
55. Kim, K. *et al.* Quantum simulation of frustrated Ising spins with trapped ions. *Nature* **465,** 590–593 (2010).
56. Edwards, E. E. *et al.* Quantum simulation and phase diagram of the transverse-field Ising model with three atomic spins. *Phys. Rev. B* **82,** 060412 (2010).
57. Islam, R. *et al.* Onset of a quantum phase transition with a trapped ion quantum simulator. *Nature Commun.* **2,** 377 (2011).
58. Kim, K. *et al.* Quantum simulation of the transverse Ising model with trapped ions. *New J. Phys.* **13,** 105003 (2011).

59. Schneider, C., Porras, D. & Schaetz, T. Experimental quantum simulations of many-body physics with trapped ions. *Rep. Prog. Phys.* **75,** 024401 (2012).
60. Lin, G-D., Monroe, C. & Duan, L-M. Sharp phase transitions in a small frustrated network of trapped ion spins. *Phys. Rev. Lett.* **106,** 230402 (2011).
61. Lamata, L., León, J., Schätz, T. & Solano, E. Dirac equation and quantum relativistic effects in a single trapped ion. *Phys. Rev. Lett.* **98,** 253005 (2007).
62. Alsing, P. M., Dowling, J. P. & Milburn, G. J. Ion trap simulations of quantum fields in an expanding universe. *Phys. Rev. Lett.* **94,** 220401 (2005).
63. Menicucci, N. C. & Milburn, G. J. Single trapped ion as a time-dependent harmonic oscillator. *Phys. Rev. A* **76,** 052105 (2007).
64. Horstmann, B., Reznik, B., Fagnocchi, S. & Cirac, J. I. Hawking radiation from an acoustic black hole on an ion ring. *Phys. Rev. Lett.* **104,** 250403 (2010).
65. Menicucci, N. C., Olson, S. J. & Milburn, G. J. Simulating quantum effects of cosmological expansion using a static ion trap. *New J. Phys.* **12,** 095019 (2010).
66. Schützhold, R. *et al.* Analogue of cosmological particle creation in an ion trap. *Phys. Rev. Lett.* **99,** 201301 (2007).
67. Gerritsma, R. *et al.* Quantum simulation of the Dirac equation. *Nature* **463,** 68–71 (2010).
68. Casanova, J., Garcia-Ripoll, J. J., Gerritsma, R., Roos, C. F. & Solano, E. Klein tunneling and Dirac potentials in trapped ions. *Phys. Rev. A* **82,** 020101 (2010).
69. Schrödinger, E. Über die kräftefreie Bewegung in der relativistischen Quantenmechanik. *Sitz. Preuss. Akad. Wiss. Phys.-Math. Kl.* **24,** 418–428 (1930).
70. Klein, O. Die Reflexion von Elektronen an einem Potentialsprung nach der relativistischen Dynamik von Dirac. *Z. Phys.* **53,** 157–165 (1929).
71. Gerritsma, R. *et al.* Quantum simulation of the Klein paradox with trapped ions. *Phys. Rev. Lett.* **106,** 060503 (2011).
72. Lutterbach, L. & Davidovich, L. Method for direct measurement of the Wigner function in cavity QED and ion traps. *Phys. Rev. Lett.* **78,** 2547–2550 (1997).
73. Lougovski, P., Walther, H. & Solano, E. Instantaneous measurement of field quadrature moments and entanglement. *Eur. Phys. J. D* **38,** 423–426 (2006).
74. Wallentowitz, S. & Vogel, W. Reconstruction of the quantum mechanical state of a trapped ion. *Phys. Rev. Lett.* **75,** 2932–2935 (1995).
75. Casanova, J. *et al.* Quantum simulation of quantum field theories in trapped ions. *Phys. Rev. Lett.* **107,** 260501 (2011).
76. Brown, K. R., Clark, R. J. & Chuang, I. L. Limitations of quantum simulation examined by simulating a pairing hamiltonian using nuclear magnetic resonance. *Phys. Rev. Lett.* **97,** 050504 (2006).
77. Lanyon, B. P. *et al.* Universal digital quantum simulations with trapped ions. *Science* **334,** 57–61 (2011).
78. Nebendahl, V., Häffner, H. & Roos, C. F. Optimal control of entangling operations for trapped-ion quantum computing. *Phys. Rev. A* **79,** 012312 (2009).
79. Barreiro, J. T. *et al.* An open-system quantum simulator with trapped ions. *Nature* **470,** 486–491 (2011).
80. Ospelkaus, C. *et al.* Trapped-ion quantum logic gates based on oscillating magnetic fields. *Phys. Rev. Lett.* **101,** 090502 (2008).
81. Johanning, M. *et al.* Individual addressing of trapped ions and coupling of motional and spin states using rf radiation. *Phys. Rev. Lett.* **102,** 073004 (2009).
82. Ospelkaus, C. *et al.* Microwave quantum logic gates for trapped ions. *Nature* **476,** 181–184 (2011).
83. Khromova, A. *et al.* A designer spin-molecule implemented with trapped ions in a magnetic gradient. Preprint at http://arxiv.org/abs/1112.5302 (2011).
84. Wang, S. X., Labaziewicz, J., Ge, Y., Shewmon, R. & Chuang, I. L. Individual addressing of ions using magnetic field gradients in a surface-electrode ion trap. *Appl. Phys. Lett.* **94,** 094103 (2009).
85. Welzel, J. *et al.* Designing spin–spin interactions with one and two dimensional ion crystals in planar micro traps. *Eur. Phys. J. D* **65,** 285–297 (2011).
86. Dubin, D. H. E. Theory of structural phase transitions in a trapped Coulomb crystal. *Phys. Rev. Lett.* **71,** 2753–2756 (1993).
87. Fishman, S., De Chiara, G., Calarco, T. & Morigi, G. Structural phase transitions in low-dimensional ion crystals. *Phys. Rev. B* **77,** 064111 (2008).
88. Lin, G-D. *et al.* Large-scale quantum computation in an anharmonic linear ion trap. *Europhys. Lett.* **86,** 60004 (2009).
89. Schaetz, T., Friedenauer, A., Schmitz, H., Petersen, L. & Kahra, S. Towards (scalable) quantum simulations in ion traps. *J. Mod. Opt.* **54,** 2317–2325 (2007).
90. Chiaverini, J. & Lybarger, J, W. E. Laserless trapped-ion quantum simulations without spontaneous scattering using microtrap arrays. *Phys. Rev. A* **77,** 022324 (2008).
91. Clark, R. J., Lin, T., Brown, K. R. & Chuang, I. L. A two-dimensional lattice ion trap for quantum simulation. *J. App. Phys.* **105,** 013114 (2009).
92. Schmied, R., Wesenberg, J. H. & Leibfried, D. Optimal surface-electrode trap lattices for quantum simulation with trapped ions. *Phys. Rev. Lett.* **102,** 233002 (2009).
93. Kumph, M., Brownnutt, M. & Blatt, R. Two-dimensional arrays of radio-frequency ion traps with addressable interactions. *New J. Phys.* **13,** 073043 (2011).
94. Schmied, R., Wesenberg, J. H. & Leibfried, D. Quantum simulation of the hexagonal Kitaev model with trapped ions. *New J. Phys.* **13,** 115011 (2011).
95. Porras, D., Marquardt, F., von Delft, J. & Cirac, J. I. Mesoscopic spin-boson models of trapped ions. *Phys. Rev. A* **78,** 010101 (2008).
96. Porras, D. & Cirac, J. I. Bose–Einstein condensation and strong-correlation behavior of phonons in ion traps. *Phys. Rev. Lett.* **93,** 263602 (2004).
97. Porras, D. & Cirac, J. I. Quantum manipulation of trapped ions in two dimensional Coulomb crystals. *Phys. Rev. Lett.* **96,** 250501 (2006).
98. Bermudez, A., Schätz, T. & Porras, D. Synthetic gauge fields for vibrational excitations of trapped ions. *Phys. Rev. Lett.* **107,** 150501 (2011).
99. Brown, K. R. *et al.* Coupled quantized mechanical oscillators. *Nature* **471,** 196–199 (2011).
100. Harlander, M., Lechner, R., Brownnutt, M., Blatt, R. & Hänsel, W. Trapped-ion antennae for the transmission of quantum information. *Nature* **471,** 200–203 (2011).
101. Schmied, R., Roscilde, T., Murg, V., Porras, D. & Cirac, J. I. Quantum phases of trapped ions in an optical lattice. *New. J. Phys.* **10,** 045017 (2008).
102. Müller, M., Liang, L., Lesanovsky, I. & Zoller, P. Trapped Rydberg ions: From spin chains to fast quantum gates. *New J. Phys.* **10,** 093009 (2008).
103. Schmidt-Kaler, F. *et al.* Rydberg excitation of trapped cold ions: A detailed case study. *New J. Phys.* **13,** 075014 (2011).
104. Mitchell, T. B. *et al.* Direct observations of structural phase transitions in planar crystallized ion plasmas. *Science* **282,** 1290–1293 (1998).
105. Sawyer, B. C. *et al.* Spectroscopy and thermometry of drumhead modes in a mesoscopic trapped-ion crystal using entanglement. Preprint at http://arxiv.org/abs/1201.4415 (2012).
106. Schneider, C., Enderlein, M., Huber, T. & Schaetz, T. Optical trapping of an ion. *Nature Photon.* **4,** 772–775 (2010).
107. Pruttivarasin, T., Ramm, M., Talukdar, I., Kreuter, A. & Häffner, H. Trapped ions in optical lattices for probing oscillator chain models. *New J. Phys.* **13,** 075012 (2011).
108. Benassi, A., Vanossi, A. & Tosatti, E. Nanofriction in cold ion traps. *Nature Commun.* **2,** 236 (2011).
109. Zipkes, C., Palzer, S., Sias, C. & Köhl, M. A trapped single ion inside a Bose–Einstein condensate. *Nature* **464,** 388–391 (2010).
110. Schmid, S., Härter, A. & Denschlag, J. H. Dynamics of a cold trapped ion in a Bose–Einstein condensate. *Phys. Rev. Lett.* **105,** 133202 (2010).
111. Aspuru-Guzik, A., Dutoi, A. D., Love, P. J. & Head-Gordon, M. Simulated quantum computation of molecular energies. *Science* **309,** 1704–1707 (2005).
112. Hauke, P., Cucchietti, F. M., Tagliacozzo, L., Lewenstein, M. & Deutsch, I. On the robustness of quantum simulators. Preprint at http://arxiv.org/abs/1109.6457 (2011).
113. Lidar, D. A., Chuang, I. L. & Whaley, K. B. Decoherence-free subspaces for quantum computation. *Phys. Rev. Lett.* **81,** 2594–2597 (1998).
114. Viola, L., Knill, E. & Lloyd, S. Dynamical decoupling of open quantum systems. *Phys. Rev. Lett.* **82,** 2417–2421 (1999).
115. Bennett, C. H., DiVincenzo, D. P., Smolin, J. A. & Wootters, W. K. Mixed-state entanglement and quantum error correction. *Phys. Rev. A* **54,** 3824–3851 (1996).

Acknowledgements

We gratefully acknowledge support by the Austrian Science Fund (FWF), by the European Commission (SCALA, AQUTE networks, STREP project MICROTRAP), by the Intelligence Advanced Research Projects Activity and by the Institut für Quanteninformation GmbH.

Additional information

The authors declare no competing financial interests. Reprints and permissions information is available online at www.nature.com/reprints. Correspondence and requests for materials should be addressed to R.B.